



Universiteit  
Leiden  
The Netherlands

## Immunosuppression in breast cancer: a closer look at regulatory T cells

Kos, K.

### Citation

Kos, K. (2023, January 11). *Immunosuppression in breast cancer: a closer look at regulatory T cells*. Retrieved from <https://hdl.handle.net/1887/3505617>

Version: Publisher's Version

License: [Licence agreement concerning inclusion of doctoral thesis in the Institutional Repository of the University of Leiden](#)

Downloaded from: <https://hdl.handle.net/1887/3505617>

**Note:** To cite this publication please use the final published version (if applicable).



# 6

## Immune checkpoint blockade triggers T<sub>reg</sub> activation which blunts therapeutic response in metastatic breast cancer

Kevin Kos<sup>1,2,3,†</sup>, Lorenzo Spagnuolo<sup>1,2†</sup>, Olga Blomberg<sup>1,2,3†</sup>, Kelly Kersten<sup>1</sup>, Cheei-Sing Hau<sup>1,2</sup>, Kim Vrijland<sup>1,2</sup>, Daphne Kaldenbach<sup>1,2</sup>, Elisabeth A.M. Raeven<sup>1,2</sup>, Karin E. de Visser<sup>1,2\*</sup>

### **Affiliations**

<sup>1</sup> Division of Tumor Biology & Immunology, Netherlands Cancer Institute, 1066 CX Amsterdam, The Netherlands

<sup>2</sup> Oncode Institute, Utrecht, The Netherlands

<sup>3</sup> Department of Immunology, Leiden University Medical Center, Leiden, The Netherlands.

<sup>†</sup> These authors contributed equally

\*Corresponding author. Email: [k.d.visser@nki.nl](mailto:k.d.visser@nki.nl)

*Unpublished*

## ABSTRACT

Immune checkpoint inhibitors such as anti-PD-1 and anti-CTLA4 are aimed at activating anti-tumoral effector cells, but their effect on immunosuppressive regulatory T cells that express high levels of immune checkpoint molecules is unclear. Using mouse models for spontaneous primary and metastatic breast cancer, we studied how immune checkpoint blockade (ICB) influences  $T_{\text{regs}}$  and how this impacts the therapeutic benefit of ICB. We observed that ICB drives intratumoral and systemic accumulation of  $T_{\text{regs}}^+$ , but not  $CD8^+$  T cells. Neoadjuvant depletion of  $T_{\text{regs}}$  combined with ICB changes the immune landscape of mammary tumors into a state favourable for ICB response, characterised by increased T-cell activation, more eosinophils, and elevated PD-L1 and MHC-II expression on myeloid cells. Systemically, depletion of  $T_{\text{regs}}$  during ICB resulted in the accumulation of  $CD8^+$  T cells and NK cells, and induces durable T cell activation. Consequently, depletion of  $T_{\text{regs}}$  in the context of ICB prolongs metastasis-related survival, which is not observed upon  $T_{\text{reg}}$  depletion or ICB alone. Combined, this study shows that  $T_{\text{regs}}$  are inadvertently activated by ICB and pose a barrier for ICB efficacy in breast cancer.

## INTRODUCTION

The development of immune checkpoint inhibitors that block immunoregulatory receptors like PD-1 and CTLA4 have ushered in a new era of cancer treatment. In particular patients with immunogenic tumors, such as melanoma<sup>1</sup>, non-small cell lung cancer (NSCLC)<sup>2</sup>, or microsatellite instable cancers<sup>3</sup>, have shown impressive responses upon treatment with anti-PD1/PD-L1 and anti-CTLA4 antibodies. However, despite these successes, an important fraction of those patients does not respond to anti-PD1 and/or anti-CTLA4 immunotherapy (ICB), or acquires treatment resistance<sup>4</sup>. Moreover, the efficacy of ICB in other cancer types, such as breast cancer, is limited<sup>5,6</sup>, highlighting the need to understand the obstacles of immunotherapy response.

The main rationale of ICB is to improve the capacity of tumor-specific CD8<sup>+</sup> T cells to expand, recognize and clear cancer cells<sup>7</sup>. To achieve this, anti-CTLA4 blocks the interaction between the co-inhibitory molecule CTLA4 expressed on T cells and CD80/CD86 expressed on mature, antigen presenting dendritic cells thereby improving T cell priming and activation. Anti-PD1 blocks the interaction of PD-1 with PD-L1, which can be widely expressed on tumor-, stromal, and immune cells and is a negative regulator of T cell function through inhibition of co-stimulation and TCR signalling<sup>8</sup>. PD-1 and CTLA-4 expression is not limited to cytotoxic CD8<sup>+</sup> T cells, but is also found on intratumoral CD4<sup>+</sup>FOXP3<sup>+</sup> regulatory T cells (T<sub>regs</sub>)<sup>9,10</sup>. T<sub>regs</sub> are important regulators of immune homeostasis endowed with a plethora of immunoregulatory features, making them key orchestrators of cancer-associated immunosuppression<sup>11,12</sup>. T<sub>regs</sub> can negatively impact anti-tumor immunity in breast cancer mouse models through inhibition of both innate and adaptive immune cell function<sup>11</sup>, thereby contributing to primary tumor growth<sup>13,14</sup> and metastases<sup>15</sup>.

Recent evidence indicates that anti-PD1 and anti-CTLA4 may inadvertently lead to the activation of T<sub>regs</sub>. Anti-PD1 has been shown to induce the proliferation of T<sub>regs</sub> in tumors of melanoma patients, which correlates to poor prognosis<sup>16</sup>. Moreover, high PD-1 expression on T<sub>regs</sub> versus CD8<sup>+</sup> T cells strongly correlates with non-responsiveness to anti-PD1 in NSCLC, gastric cancer and melanoma patients<sup>17</sup>, and has been linked to hyper progression in gastric cancer patients<sup>18</sup>. Anti-CTLA4 was found to induce proliferation of tumor-associated T<sub>regs</sub> in MC38 tumor-bearing mice<sup>19</sup>. In cancer patients, anti-CTLA4 treatment has been shown to expand immunosuppressive T<sub>regs</sub> in blood and tumors<sup>20,21</sup>, although it is unclear how this impacts therapy response. These data suggest that activation of T<sub>regs</sub> might be an unintended effect of ICB, raising the question how this impacts the anti-cancer efficacy of ICB.

Here, we set out to study whether interactions between T<sub>regs</sub> and dual anti-PD1 and anti-CTLA4 blockade form a hurdle for anti-tumor immunity. To study this, we made use of the transgenic *K14cre;Cdh1<sup>F/F</sup>;Trp53<sup>F/F</sup>* (KEP) mouse model of invasive mammary tumorigenesis<sup>22</sup>, and the KEP-based mastectomy model for spontaneous multi-organ metastatic disease<sup>23</sup>. Primary

tumors and metastases arising in these models are unresponsive to ICB. We observed that ICB fails to induce CD8<sup>+</sup> T cell activation or proliferation, but instead enhance T<sub>reg</sub> proliferation and activation in tumor-bearing mice. Neoadjuvant ablation of T<sub>regs</sub> using the *Foxp3*<sup>DTR-GFP</sup> model in the context of ICB led to the accumulation of CD8<sup>+</sup> T cells, eosinophils and NK cells in blood. Strikingly, ICB synergizes with T<sub>reg</sub> depletion to curb metastatic disease. Combined, this study provides experimental evidence that T<sub>regs</sub> impair the efficacy of ICB in spontaneous models for breast cancer.

## RESULTS

### ICB drives T<sub>reg</sub> accumulation in ICB-unresponsive spontaneous mammary tumors

To investigate the impact of T<sub>regs</sub> on immunotherapy response, we first assessed the efficacy of dual anti-PD1 anti-CTLA4 immune checkpoint blockade in controlling tumor growth of transgenic KEP mice bearing spontaneous mammary tumors. Treatment with ICB was initiated at a tumor size of 25mm<sup>2</sup> and continued until end-stage tumor size (225mm<sup>2</sup>) was reached (Fig. 1A). Consistent with poor ICB response in breast cancer patients, ICB treatment did not enhance survival of tumor-bearing KEP mice compared to control treatment (Fig. 1B). Characterisation of T cell populations in tumors of KEP mice showed that ICB treatment does not alter the intratumoral infiltration of CD8<sup>+</sup> and CD4<sup>+</sup> T cells (Fig. S1A), but instead increased the intratumoral accumulation of FOXP3<sup>+</sup> cells (Fig. 1C, D). As a result, the intratumoral ratio of CD8/FOXP3 cells decreased upon ICB treatment (Fig. S1B), whereas a high CD8/FOXP3 ratio has been associated with improved survival in breast cancer patients<sup>24</sup>. In line with increased intratumoral accumulation of FOXP3<sup>+</sup> cells, we found increased expression of the proliferation marker Ki-67 on T<sub>regs</sub> in KEP mice treated with ICB compared to untreated mice (Fig. 1E). Next, we investigated whether the observed increase in T<sub>regs</sub> in ICB-treated mice was limited to the TME by analysing blood and lymph nodes of ICB-treated KEP mice bearing end-stage tumors. This showed that T<sub>regs</sub>, but not CD8<sup>+</sup> T cells, are also increased in blood of tumor-bearing KEP mice receiving ICB (Fig. 1G, S1C). In tumor-draining lymph nodes, T<sub>reg</sub> frequency was not significantly altered, but these T<sub>regs</sub> did express higher levels of Ki-67 (Fig. S1D).

To study the impact of T<sub>regs</sub> on immunotherapy response in the context of metastasis, we first set out to validate our findings in the orthotopic KEP transplantation model, based on transplantation of tumor fragments (Fig. 1G). Similar to the spontaneous KEP model, ICB treatment does not enhance the survival of mice bearing orthotopically transplanted KEP tumors compared to control treatment (Fig. 1H). Furthermore, T<sub>regs</sub>, but not conventional T cells, were increased in frequency and showed enhanced Ki-67 expression in tumors of ICB-treated mice, compared to control-treated mice (Fig. 1I-J, S1E). Finally, in these mice, T<sub>regs</sub> in blood were found to be increased upon ICB treatment (Fig. 1K), in line with observations in the spontaneous KEP model (Fig. 1F). To evaluate whether ICB, besides T<sub>reg</sub> accumulation, also influences T<sub>reg</sub> functionality *in*

*in vitro*, a suppression assay was performed. T<sub>regs</sub> isolated from draining lymph nodes of control-, or ICB-treated KEP tumor-bearing mice were co-cultured with *in vitro* activated splenic T cells to assess the impact of either T<sub>reg</sub> population on T cell proliferation. Both T<sub>reg</sub> populations similarly inhibited the proliferation of responder T cells, demonstrating that ICB does not enhance the suppressive capacity of T<sub>regs</sub> in this *ex vivo* context (Fig. 1L). Combined, these data show that ICB induces systemic accumulation of T<sub>regs</sub> in tumor-bearing mice, raising the question how this impacts immune cell crosstalk in ICB-treated mice.

### Neoadjuvant depletion of T<sub>regs</sub> in the context of ICB remodels systemic and tumor immune landscapes

To gain insight into the function of T<sub>regs</sub> in the context of ICB, we utilized *Foxp3*<sup>DTR-GFP</sup> mice that we generated on the FVB genetic background in which T<sub>regs</sub> can be transiently depleted upon short-term diphtheria toxin (DT) treatment<sup>25</sup>. *Foxp3*<sup>DTR-GFP</sup> mice were transplanted with KEP tumor fragments, and upon tumor take, mice were treated with combinations of ICB, ICB control antibody (rat IgG2a clone 2A3), DT, or PBS (DT vehicle control), until tumors reached a size of ~120mm<sup>2</sup> (Fig. 2A). At this time point, mastectomy was performed to remove the primary tumor. Analysis of blood and resected tumors showed that T<sub>regs</sub> were efficiently depleted from mice treated with DT and ICB + DT (Fig. S2A, 2G).

First, we investigated whether depletion of T<sub>regs</sub> in the context of ICB changes the composition and activation of circulating immune cells, measured 1-2 days before mastectomy (pre-mastectomy). Interestingly, besides their effect on T<sub>regs</sub>, both ICB and DT monotherapy do not significantly impact the immune cell abundance in blood compared to control-treated mice, with the exception of increased eosinophil counts upon DT treatment (Fig. 2B, S2B). In contrast, the combination of ICB and DT induced a significant increase in both CD8<sup>+</sup> T cells and NK cells compared to monotherapies (Fig. 2C-D), both of which are important effector cells for anti-tumor immunity. Notably, we also observed a strong increase in CD4<sup>+</sup>CD8<sup>+</sup> T cells (Fig. 2E), which have been described to be enriched in patients with auto-immune disease<sup>26,27</sup> and cancer<sup>28,29</sup>, and have been shown to display reactivity towards autologous melanoma cell lines *in vitro*<sup>29</sup>. As genetic ablation of T<sub>regs</sub> is associated with the development of autoimmune-related pathology<sup>30,31</sup>, we performed a preliminary analysis to investigate whether combining ICB with T<sub>reg</sub> depletion exacerbates inflammation-related pathology compared to T<sub>reg</sub>-depleted mice. Histopathological assessment of various tissues obtained from mice that were sacrificed after mastectomy at indicated time points was performed blindly by a trained animal pathologist. This revealed no differences in inflammation-related pathology between control + DT and ICB + DT treatment groups (Fig. S2C, Table 1). In addition, no differences were observed in sizes of spleen, and small intestine (S2D). Due to the preliminary nature of this investigation, further analysis in tumor- and non-tumor bearing mice with matched duration of control-, ICB- and DT treatment, should clarify to what extent the observed pathology is explained by cancer-related inflammation as opposed to T<sub>reg</sub> depletion-induced inflammation.

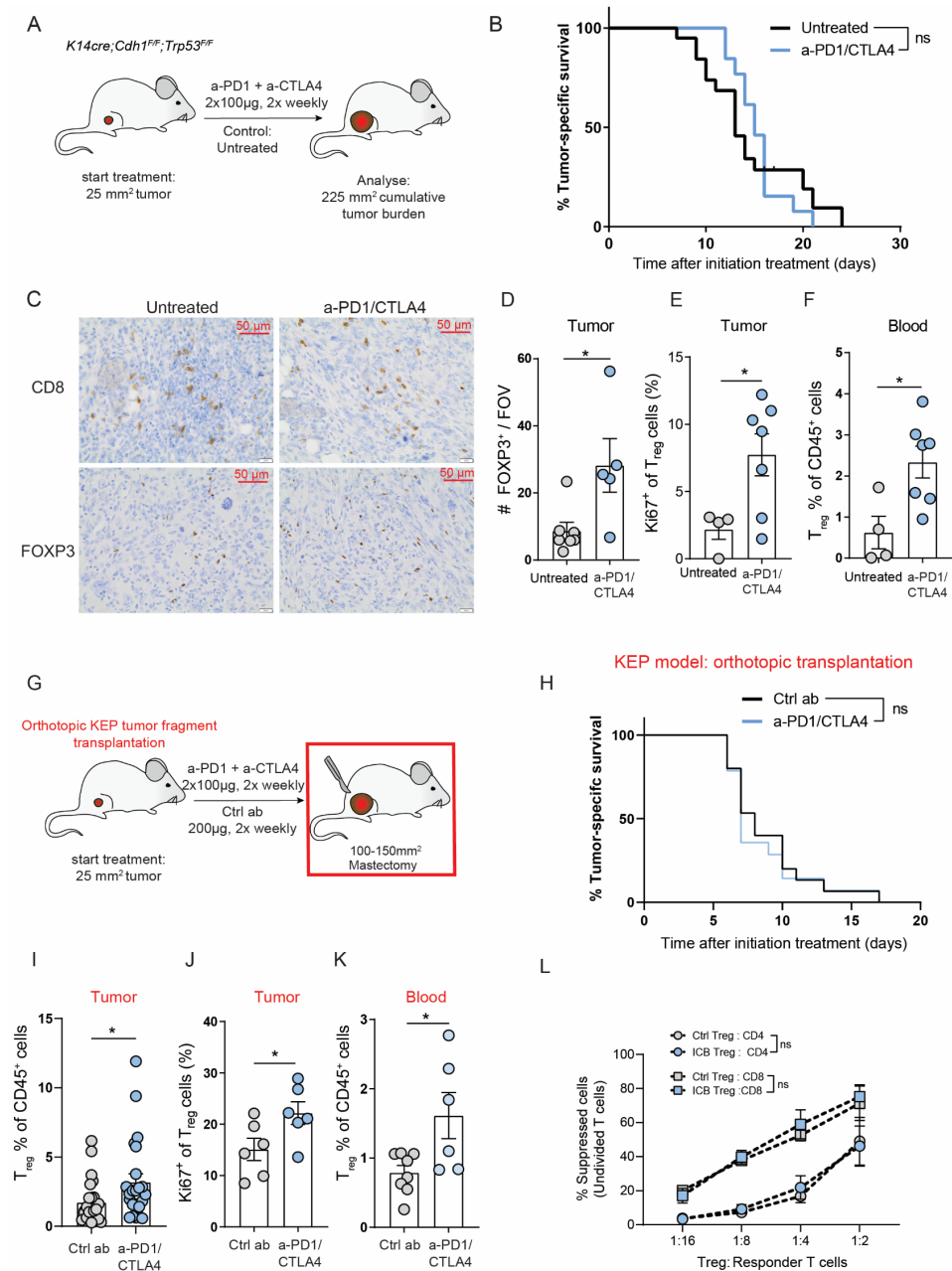


**FIGURE 1. ICB fails to inhibit mammary tumor outgrowth and activates intratumoral and systemic  $T_{reg}$  accumulation in transgenic KEP mice**

**A.** Schematic overview of study: tumor-bearing KEP mice either did not receive treatment, or were treated with a combination of anti-PD-1 and anti-CTLA4 (ICB) starting at a tumor size of 25mm<sup>2</sup> until end stage tumor size of 225mm<sup>2</sup>. **B.** Kaplan-Meier survival curves of KEP mice treated as indicated (n= 12-15 mice/group). Censored cases indicate mice that were sacrificed due to tumor-unrelated causes. **C.** Representative images of immunohistochemical staining of CD8 and FOXP3 in mammary tumors (225mm<sup>2</sup>) of KEP mice, treated as indicated. Scale bar of 50  $\mu$ m is shown. **D.** FOXP3 counts in spontaneous mammary tumors



(225mm<sup>2</sup>) of KEP mice treated as indicated, as determined by immunohistochemical analysis (counts per 40x field of view, average of five randomly selected areas) (n=5-7 mice/group). **E.** Frequency of Ki-67 expression on T<sub>regs</sub> (CD4<sup>+</sup>CD25<sup>+</sup>) in mammary tumors (225mm<sup>2</sup>) of untreated or anti-PD-1/CTLA4-treated KEP mice, analysed by flow cytometry (n=4-7 mice/group). **F.** Frequency of T<sub>regs</sub> (CD4<sup>+</sup>CD25<sup>+</sup>) as % of total live CD45<sup>+</sup> cells in blood of untreated or anti-PD-1/CTLA4-treated KEP mice bearing mammary tumors (225mm<sup>2</sup>) as determined by flow cytometry (n=4-7 mice/group). **G.** Schematic overview of study: mice bearing orthotopically transplanted KEP tumors fragments (1mm<sup>2</sup>) were treated twice weekly with control antibody or a combination of anti-PD-1 and anti-CTLA4 (ICB) starting at a tumor size of 25mm<sup>2</sup>. **H.** Kaplan-Meier survival curve of mice bearing orthotopically transplanted KEP tumors that were treated with control antibody (n=15) or ICB (n=14). Endpoint was defined as tumor size of 12x12mm<sup>2</sup>. **I.** Frequency of T<sub>regs</sub> as % of total live CD45<sup>+</sup> cells in orthotopically transplanted KEP tumors (100-150mm<sup>2</sup>) of mice treated with control antibody, or anti-PD-1/CTLA4, as analysed by flow cytometry (n=23-24 mice/group). **J.** Frequency of Ki-67 expression on T<sub>regs</sub> in orthotopically transplanted KEP tumors (100-150mm<sup>2</sup>) of mice treated with control antibody, or anti-PD-1/CTLA4, as analysed by flow cytometry (n=4-7 mice/group). **K.** Frequency of T<sub>regs</sub> as % of total live CD45<sup>+</sup> cells in blood of mice bearing orthotopically transplanted KEP tumors treated with control antibody, or anti-PD-1/CTLA4, 1-2 days before mastectomy, as analysed by flow cytometry (n=4-7 mice/group). **L.** Quantification of undivided responder cells (CD8<sup>+</sup> and CD4<sup>+</sup> T cells) based on flow cytometric assessment of CTV dilution, upon co-culture with CD3/CD28 pre-activated T<sub>regs</sub> (CD4<sup>+</sup>CD25<sup>+</sup>) isolated from lymph nodes of mice bearing transplanted mammary tumors (225mm<sup>2</sup>). Mice were treated with control antibody or anti-PD-1/CTLA4. Cells were co-cultured at indicated ratios for 96h in presence of CD3/CD28 beads (data pooled from 2 independent *in vitro* experiments, with n=4 biological replicates).

Data in D-F, I-L show mean ± SEM. P-values are determined by Log-rank test (B), Unpaired Students T-test (D-F, I-L). \* P < 0.05, \*\* P < 0.01, \*\*\* P < 0.001, \*\*\*\* P < 0.0001.

To assess potential changes in CD8<sup>+</sup> T cell activation that occur upon treatment with ICB and DT, the expression of CD44, CD62L, PD-1, CD25, CD69 was measured in blood of tumor-bearing mice by flow cytometry. T<sub>reg</sub> depletion was sufficient to strongly increase the frequency of CD44<sup>+</sup>CD62L<sup>-</sup> effector cells as compared to ICB and control-treated mice, which is not further increased upon combination of ICB + DT. Only the frequency of PD-1 was further increased on CD8<sup>+</sup> T cells upon the combination of ICB and DT compared to DT alone (Fig. 2F). Similar observations were made for CD4<sup>+</sup> T cells (S2E). Combined, these data show that T<sub>reg</sub> depletion is sufficient to induce CD8<sup>+</sup> T cell activation in blood, but the combination of ICB + DT is necessary to increase circulating CD8<sup>+</sup> T cells and NK cells.

Analysis of the immune landscape in resected tumors showed that none of the treatments altered the frequency of conventional T cells as measured by flow cytometry. Notably, T<sub>reg</sub> depletion, either with or without ICB, did induce changes in the myeloid compartment (Fig. 2G). In line with previous research, we observed that T<sub>reg</sub> depletion promoted an increase in eosinophil<sup>32</sup> and a decrease in cDC2 tumor infiltration<sup>33</sup> (Fig. 2G). Thus, in contrast to blood, changes in immune cell composition in resected tumors are mostly dictated by T<sub>reg</sub> ablation, and are not further changed upon combination of ICB and DT (Fig. 2H). Similarly, the intratumoral accumulation of activated CD8<sup>+</sup> and CD4<sup>+</sup> T cells is enhanced upon T<sub>reg</sub> depletion compared to control, and ICB + DT compared to ICB alone (Fig. 2H, S2F). However, besides upregulation of CD69 on CD8<sup>+</sup> T cells, the combination of ICB + DT does not further enhance the intratumoral accumulation activated T cells compared to control + DT (Fig. 2H, S2G).

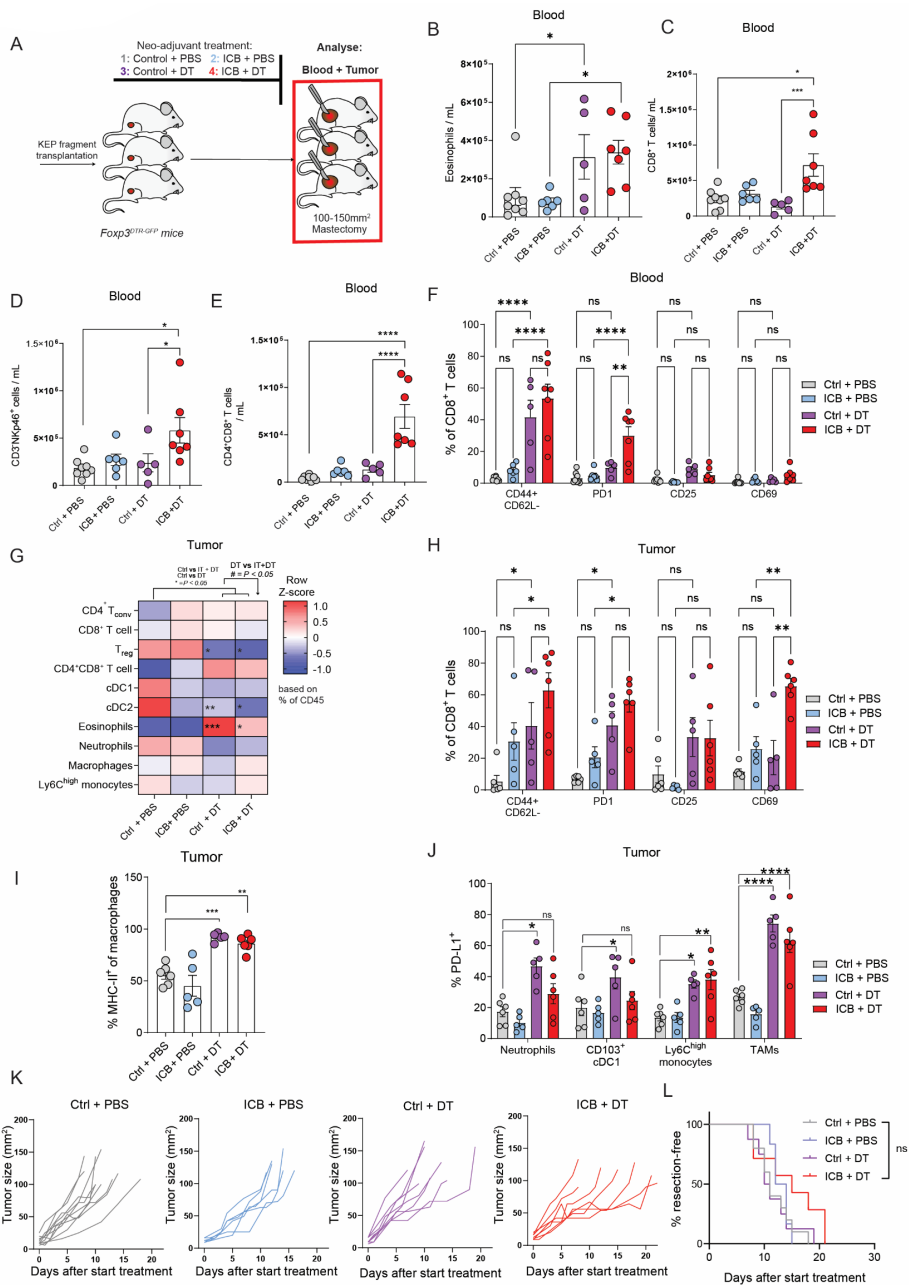


**FIGURE 2. Neoadjuvant depletion of T<sub>regs</sub> changes the systemic and tumor immune landscape, but does not improve ICB response in primary tumors**

**A.** Schematic overview of study. KEP-tumor fragments were orthotopically transplanted, and mice were treated with combinations of ICB, control antibody (rat IgG2a, clone 2A3), DT or PBS (DT vehicle control) as indicated. Ctrl or ICB was started upon presentation of palpable tumors (4-6mm<sup>2</sup>), administered twice weekly, and discontinued upon mastectomy. DT or PBS was started at a tumor size of 9-12 mm<sup>2</sup> and administered twice in total (day 0 & 4). At a tumor size of 100-150mm<sup>2</sup>, mastectomy

was performed. Blood (taken 1-2 days before mastectomy) and resected tumors were analysed by flow cytometry. **B-E.** Absolute cell counts of eosinophils (B) CD8<sup>+</sup> T cells (C), NK cells (D) and CD4<sup>+</sup>CD8<sup>+</sup> T cells (E) in blood of mice treated with indicated treatments, as determined by flow cytometry, 1-2 days before mastectomy (n=5-8 mice/group). **F.** Frequency of indicated markers (% of positive cells) gated on CD8<sup>+</sup> T cells in blood of mice treated with indicated treatments, as determined by flow cytometry, 1-2 days before mastectomy (n=5-8 mice/group). **G.** Heatmap depicting tumor-immune landscape in mastectomized tumors of mice receiving indicated treatments. Row Z-score calculated based on frequency of indicated cell type of total CD45<sup>+</sup> cells (n=5-6 mice/group). **H.** Frequency of indicated markers (% of positive cells) gated on CD8<sup>+</sup> T cells in mastectomized tumors of mice treated with indicated treatments, as determined by flow cytometry (n=5-6 mice/group). **I.** Frequency of MHC-II<sup>+</sup> cells gated on macrophages (CD11b<sup>+</sup> F4/80<sup>+</sup>) in mastectomized tumors of mice receiving indicated treatments (n=5-6 mice/group). **J.** Frequency of PD-L1<sup>+</sup> cells within indicated immune cell subsets in mastectomized tumors of mice receiving indicated treatments (n=5-6 mice/group). **K.** Tumor growth curves of individual mice receiving indicated treatments (n=6-10 mice/group). **L.** Kaplan-Meier curve of mice bearing orthotopically transplanted KEP tumors treated as indicated. Endpoint was reached when mice underwent mastectomy at ~120mm<sup>2</sup> (n=7-10 mice/group).

Data in B-F,H-J show mean ± SEM. P-values were calculated by One-way ANOVA with Sidak's correction (B-E, G), Tukey's correction, Holm-Sidak correction (G). 2-way ANOVA with Sidak correction (F,H, J), Log-rank test (L). \* P < 0.05, \*\* P < 0.01, \*\*\* P < 0.001, \*\*\*\* P < 0.0001

In addition to these observations, we found that T<sub>reg</sub> depletion upregulated PD-L1 expression on neutrophils, conventional dendritic cells (cDC1), Ly6C<sup>high</sup> monocytes and tumor-associated macrophages (TAMs) (Fig. 2J). Importantly, PD-L1 is a clinical biomarker for response to immune-checkpoint inhibitors, suggesting that T<sub>reg</sub> depletion may remodel the TME into a state that is favourable for ICB response. We also found a strong increase of MHC-II expression on TAMs, reflective of M1-like polarization based on this single marker, to which anti-tumoral functions have been attributed<sup>34</sup> (Fig. 2I). Importantly, these changes were not further enhanced in the context of ICB. One change in tumors that was associated to the combination of ICB + DT, but not control + DT is an increase in frequency of inflammatory CD101<sup>+</sup>CD62L<sup>-</sup> eosinophils, as compared to control treatment (Fig. S2). Together, this shows that genetic ablation of T<sub>regs</sub> drives broad pro-inflammatory changes in intratumoral T- and myeloid cells. These changes are mostly related to T<sub>reg</sub> depletion and occur independent of ICB, despite the observation that ICB increases the intratumoral accumulation of T<sub>regs</sub>. Finally, analysis of tumor sizes revealed that none of the treatments significantly delayed tumor growth (Fig. 2K-L), showing that depletion of T<sub>regs</sub> in the context of ICB does not drive anti-tumor responses. These findings are in line with previous results showing that T<sub>regs</sub> are not critical for regulation of primary tumor growth in the KEP model<sup>15</sup>.

**TABLE 1.** Histopathological assessment of immune-related pathology in mice receiving neoadjuvant treatment with Ctrl + DT and ICB + DT, as analysed blindly by a trained pathologist, related to figure S2C. Mice were sacrificed at indicated time points after mastectomy due to development of metastasis- or metastasis-unrelated pathology (see Table 2)

Case #	Exp group	Tumor-draining axillary lymph node	Non-draining axillary lymph node	Spleen	Pancreas	Lungs	Liver	Kidneys
21KDV930	Ctrl + DT	Lymphocytic hyperplasia	Marked hyperplasia with lymphocytes and plasma cells	Lymphoid compartment: apoptotic lymphocytes, moderate numbers	Marked neutrophilic interstitial pancreatitis, with atrophy/loss of exocrine pancreatic tissue (60% affected)	Moderate inflammation, mostly perivascular lymphocytic Focal small cluster of cells resembling (metastatic) carcinoma	Moderate inflammation, mostly adjacent to central veins and bile ducts / portal areas, with neutrophils, lymphocytes, plasma cells	Mild multifocal interstitial nephritis with neutrophils, macrophages, lymphocytes, plasma cells
21KDV696	Ctrl + DT	Lymphocytic hyperplasia	No abnormalities	Lymphoid compartment: apoptotic lymphocytes, moderate numbers	Marked subacute interstitial pancreatitis, with neutrophils, lymphocytes and plasma cells, degeneration and atrophy/loss of exocrine pancreatic tissue (30% affected)	Moderate inflammation, mostly perivascular lymphocytic	Moderate inflammation, mostly adjacent to central veins and bile ducts / portal areas, with neutrophils, lymphocytes, plasma cells	Mild multifocal interstitial nephritis with neutrophils, macrophages, lymphocytes, plasma cells
21VIS010	Ctrl + DT	Minimal lymphocytic hyperplasia	Hyperplastic	Lymphoid compartment: apoptotic lymphocytes, low numbers	-	Carcinoma metastases in pleura and lung	Moderate inflammation, mostly adjacent to central veins and bile ducts / portal areas, with neutrophils, lymphocytes, plasma cells	Minimal focal interstitial nephritis
21VIS012	Ctrl + DT	No abnormalities	Hyperplastic, with many apoptotic lymphocytes	Mild lymphocytic hyperplasia, moderate numbers of apoptotic lymphocytes	Marked subacute interstitial pancreatitis, with neutrophils, lymphocytes and plasma cells, degeneration and atrophy/loss of exocrine pancreatic tissue (50% affected)	Mild inflammation, mostly perivascular lymphocytic Focal small cluster of cells resembling (metastatic) carcinoma	Mild inflammation, mostly adjacent to central veins and bile ducts / portal areas, with neutrophils, lymphocytes, plasma cells	Minimal focal interstitial nephritis

TABLE 1 CONTINUED.

Case #	Exp group	Tumor-draining axillary lymph node	Non-draining axillary lymph node	Spleen	Pancreas	Lungs	Liver	Kidneys
21KDV388	ICB + DT 10 days after mastectomy	Hyperplastic, many apoptotic cells, multifocal lymphadenitis with neutrophils, macrophages and multinucleated giant cells	Hyperplastic, with many apoptotic lymphocytes	Lymphoid compartment: hyperplasia, many apoptotic lymphocytes	Moderate interstitial pancreatitis, mostly periductal, with neutrophils, lymphocytes and plasma cells (20% affected)	Marked vasculitis and perivascularitis with many lymphocytes, in some places associated with local crystalline macrophage pneumonia	Moderate inflammation, mostly adjacent to central veins and bile ducts / portal areas, with neutrophils, lymphocytes, plasma cells	Mild multifocal interstitial nephritis with neutrophils, macrophages, lymphocytes, plasma cells
21KDV519	ICB + DT 56 days after mastectomy	Hyperplastic, moderate numbers of apoptotic cells	No abnormalities	No abnormalities	Moderate periductal inflammation (10% affected)	Mild vasculitis and perivascularitis	Mild inflammation, mostly adjacent to central veins and bile ducts / portal areas, with neutrophils, lymphocytes, plasma cells	Mild interstitial nephritis, mild dilation of pelvis and cortical tubules
21KDV677	ICB + DT 80 days after mastectomy	Hyperplastic	Hyperplastic	Increased numbers of megakaryocytes in the hematopoietic compartment	Mild periductal inflammation (5% affected)	Minimal perivascular inflammation	Minimal inflammation, mostly adjacent to central veins and bile ducts / portal areas, with neutrophils, lymphocytes, plasma cells	Minimal focal interstitial nephritis
21KDV678	ICB + DT 80 days after mastectomy	Moderate numbers of apoptotic lymphocytes	Hyperplastic, with moderate numbers of apoptotic lymphocytes	Mild lymphoid hyperplasia, few germinal centers	Moderate periductal inflammation (40% affected)	Minimal perivascular inflammation	Mild to moderate inflammation, mostly adjacent to central veins and bile ducts / portal areas, with neutrophils, lymphocytes, plasma cells	Minimal focal interstitial nephritis and tubular degeneration

### **T<sub>reg</sub>-depletion during ICB induces durable systemic T cell activation and prolongs metastasis-related survival**

Ablation of T<sub>regs</sub> during ICB mobilised both CD8<sup>+</sup> T cells and NK cells in blood of tumor-bearing mice, raising the question whether T<sub>regs</sub> functionally impair the systemic immune activation necessary to combat metastasis. To investigate whether neoadjuvant T<sub>reg</sub> depletion in the context of ICB affects metastasis formation, mice were monitored for development of overt metastatic disease after resection of primary tumors (Fig. 3A). In addition, T cell activation was analysed in blood of mice 7 days after mastectomy (post-mastectomy). Of note, mice were only treated before resection of the primary tumor. Despite discontinuation of ICB, T<sub>regs</sub> were still found to be increased in blood of mice that had been treated with ICB before mastectomy, as measured by flow cytometry 7 days after mastectomy (Fig. 3B). Moreover, these T<sub>regs</sub> displayed increased expression of the activation markers CD44 and PD-1 compared to control-treated mice, which was not observed in the initial pre-mastectomy characterisation (Fig. 3C, S3A). Interestingly, CD44<sup>+</sup>T<sub>regs</sub> have been described to have strong immunosuppressive potential, and play an important role in curbing autoimmunity<sup>35</sup>. In addition, a recent study showed that PD-1<sup>+</sup>T<sub>regs</sub> gain increased proliferative and immunosuppressive capacity upon PD-1 blockade *in vitro*<sup>17,18</sup>. Thus, our data suggest that ICB does not only drive the expansion of T<sub>regs</sub> in blood, but on a longer-term, also induces phenotypical changes that are associated to T<sub>reg</sub> activation.

To analyse whether neoadjuvant depletion of T<sub>regs</sub> in the context of ICB induces long-term effects after discontinuation of treatment, we next assessed T cell activation in blood of mice 7 days after mastectomy. At this time point, we found that both the CD8 and CD4 T cell compartment in blood of mice that had been treated with ICB + DT before mastectomy harboured a significantly increased frequency of CD44<sup>+</sup>CD62L<sup>-</sup> effector cells, compared to control- and monotherapies (Fig. 3D, S3B). In addition, CD8<sup>+</sup>T cells in mice previously treated with ICB + DT showed increased expression of PD-1 compared to all monotherapies, and increased CD69 expression compared to control-treated mice. To further assess the kinetics of this observation, we compared CD8<sup>+</sup> T cell activation between control + DT and ICB + DT treated mice pre- and post-mastectomy (Fig. 3E). The CD44<sup>+</sup>CD62L<sup>-</sup> effector CD8 T cell population is maintained in mice that had been treated with ICB + DT before mastectomy, but is decreased in mice previously treated with control + DT (Fig. 3F). Thus, neoadjuvant systemic depletion of T<sub>regs</sub> in the context of ICB leads to durable T cell activation, at least up until 7 days after discontinuation of treatment, raising the question whether these systemic pro-inflammatory conditions may have anti-metastatic potential. Analysis of metastasis-related survival showed that control antibody-treated mice developed metastatic disease, characterised by respiratory distress and end-stage metastatic tumor burden (>225mm<sup>2</sup>) in axillary lymph nodes and intraperitoneal organs (causes of death indicated in Table 2), with a median survival of 28 days. In line with previously published results describing an important role for T<sub>regs</sub> in the development of lymph node metastasis in the KEP metastasis model<sup>15</sup>,

we did not detect any lymph node metastasis in T<sub>reg</sub>-depleted mice, either with or without ICB. Strikingly, whereas neoadjuvant ICB treatment nor neoadjuvant T<sub>reg</sub> depletion improved survival, the combined treatment of T<sub>reg</sub> depletion and ICB treatment significantly prolonged metastasis-related survival (Fig 3G). Combined, these data show that T<sub>regs</sub> form a barrier for response to ICB in a mouse model for spontaneous breast cancer metastasis.

**TABLE 2.** Cause of death of mice shown in figure 3G

Case	Treatment	Cause of death
21KDV682	Ctrl + PBS	Respiratory distress
21KDV694	Ctrl + PBS	Respiratory distress
21KDV704	Ctrl + PBS	Tumor burden lymph node metastasis + Respiratory distress
21KDV709	Ctrl + PBS	Respiratory distress
21KDV716	Ctrl + PBS	Tumor burden lymph node metastasis
21KDV722	Ctrl + PBS	Respiratory distress
21KDV773	Ctrl + PBS	Tumor burden lymph node/liver metastasis + Respiratory distress
21KDV839	Ctrl + PBS	Respiratory distress
21KDV917	Ctrl + PBS	Tumor burden intraperitoneal metastasis
21VIS011	Ctrl + PBS	Respiratory distress
21KDV369	ICB + PBS	Respiratory distress
21KDV381	ICB + PBS	Respiratory distress
21KDV391	ICB + PBS	Respiratory distress
21KDV410	ICB + PBS	Tumor burden lymph node metastasis
21KDV430	ICB + PBS	Metastasis-unrelated death
21KDV489	ICB + PBS	Respiratory distress
-	Ctrl + DT	Metastasis-unrelated death
21KDV696	Ctrl + DT	Respiratory distress
21KDV794	Ctrl + DT	Metastasis-unrelated death
21KDV801	Ctrl + DT	Respiratory distress
21KDV930	Ctrl + DT	Respiratory distress
21VIS010	Ctrl + DT	Respiratory distress
21VIS012	Ctrl + DT	Metastasis-unrelated death
22KDV032	Ctrl + DT	Long-term survivor
21KDV388	ICB + DT	Respiratory distress
21KDV443	ICB + DT	Metastasis-unrelated death
21KDV484	ICB + DT	Respiratory distress
21KDV485	ICB + DT	Respiratory distress
21KDV519	ICB + DT	Metastasis-unrelated death
21KDV677	ICB + DT	Long-term survivor
21KDV678	ICB + DT	Long-term survivor

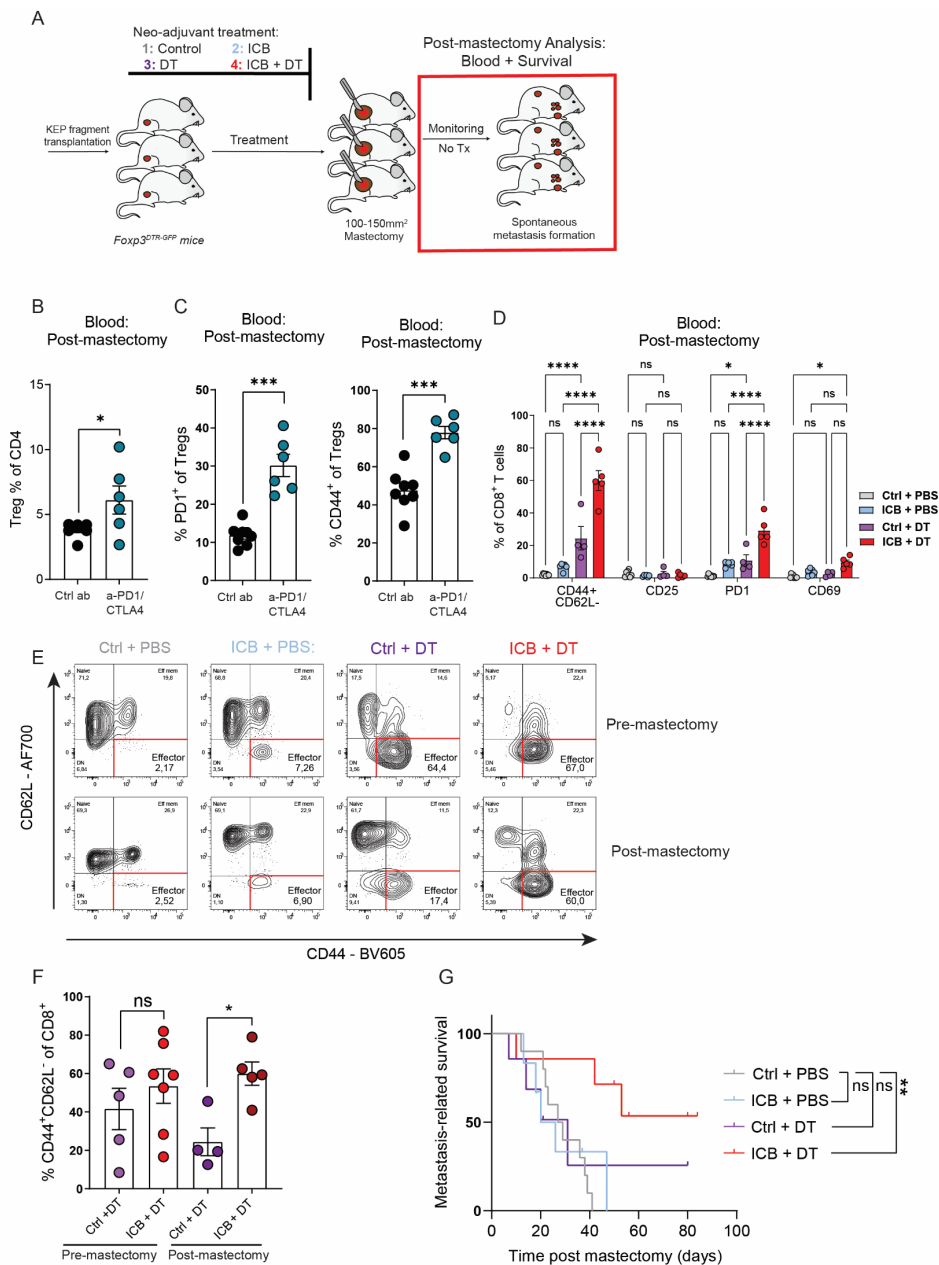


**FIGURE 3. ICB combined with T<sub>reg</sub> depletion induces durable systemic T cell activation and extends metastasis-related survival**

Mice were treated as described in figure 2A. After mastectomy, treatments were discontinued, and mice were monitored for the development of metastatic disease. Blood samples were analysed 7-8 days after (post) mastectomy by flow cytometry. **B.** Frequency of T<sub>regs</sub> (CD4<sup>+</sup>CD25<sup>+</sup>) as % of total live CD45<sup>+</sup> cells in blood of mice 7 days after mastectomy, previously treated as indicated (n=6-8 mice/group). **C.** Frequency of PD-1 (left) and CD44 (right) expression on gated T<sub>regs</sub> (CD4<sup>+</sup>CD25<sup>+</sup>) in blood of mice 7 days after mastectomy, previously treated as indicated (n=6-8 mice/group). **D.**



Frequency of indicated markers (% of positive cells) gated on CD8<sup>+</sup> T cells in blood of mice 7 days after mastectomy, previously treated as indicated (n=6-8 mice/group). **E.** Representative dot plots depicting CD44 and CD62L expression gated on CD8<sup>+</sup> T cells, in blood of mice receiving indicated neoadjuvant treatments, analysed 1-2 days before mastectomy (pre-mastectomy) and 7 days after mastectomy (post-mastectomy). **F.** Frequency of CD44<sup>+</sup>CD62L<sup>-</sup> effector cells of CD8<sup>+</sup> T cells in blood of mice receiving indicated neoadjuvant treatments, assessed pre- and post-mastectomy (n=4-7 mice/group). **G.** Kaplan-Meier plot showing metastasis-related survival after mastectomy of mice treated as indicated. Censored cases represent mice that were sacrificed due to tumor-unrelated causes (n=7-10 mice/group).

Data in B-D, F show mean ± SEM. P-values were calculated by Student's T-test (B-D,F), log-rank test (G). \* P < 0.05, \*\* P < 0.01, \*\*\* P < 0.001, \*\*\*\* P < 0.0001.

## DISCUSSION

Understanding the hurdles that impair effective anti-tumor immunity upon anti-PD-1/CTLA4 therapy is key to improve responses rates to ICB in breast cancer patients. Here, we used the clinically relevant KEP-based mouse model for spontaneous multi-organ breast cancer metastasis<sup>23</sup>, which is unresponsive to combined a-PD-1/a-CTLA4 therapy, to study how T<sub>regs</sub> impact resistance to ICB. Analysis of mammary tumor-bearing mice showed that ICB increases the accumulation of T<sub>regs</sub>, but not conventional T cells, in blood and tumors (Fig. 1). Neoadjuvant depletion of T<sub>regs</sub> during ICB induced the expansion of CD8<sup>+</sup> T cells and NK cells in blood of KEP tumor-bearing mice, which was not observed upon T<sub>reg</sub> depletion without ICB (Fig. 2). T<sub>reg</sub> depletion by itself strongly induces activation of T cells in the blood compartment, which could be significantly extended upon combination of ICB and T<sub>reg</sub> depletion (Fig. 3). This likely has consequences for metastasis formation, as the combination of T<sub>reg</sub> depletion and ICB improves metastasis-related survival compared to control-treated mice, which was not observed in mice treated with either monotherapy. Combined, these findings demonstrate that T<sub>regs</sub> can form a hurdle for response to ICB in a mouse models for spontaneous breast cancer metastasis formation.

ICB-induced accumulation and activation of T<sub>regs</sub> in tumor-bearing mice potentially enhances intratumoral and systemic immunosuppression, which may antagonize effective anti-tumor immunity. Based on the findings in our study, we propose several mechanisms that may contribute to improved control of metastases observed upon T<sub>reg</sub> depletion in the context of ICB. Interestingly, we found that T<sub>regs</sub> control several parameters that have been associated to therapeutic responses of ICB. In tumors, T<sub>reg</sub> depletion resulted in the upregulation of PD-1 on CD8<sup>+</sup> T cells, and PD-L1 on myeloid cells. Both these observations are linked to response to anti-PD-1 therapy<sup>17,36</sup>. In addition, T<sub>reg</sub> depletion re-shaped the TME into a more pro-inflammatory anti-tumorigenic environment, most notably characterized by increased infiltration of activated CD8<sup>+</sup> T cells, inflammatory eosinophils and M1-like macrophage polarization. These populations have been described to have direct tumor-killing capacities<sup>37-39</sup> and both eosinophils and M1-like macrophages promote CD8<sup>+</sup> T cell

activation, via amongst others, expression of T cell recruiting and activation chemokines such as CXCL9 and increased antigen presentation capacity<sup>40,41</sup>. Interestingly, increased systemic and intratumoral eosinophil accumulation has previously been associated with ICB response in melanoma patients<sup>42</sup> and linked to anti-tumorigenic activity in mouse models of breast cancer responsive to ICB<sup>40</sup>. Furthermore, increased recruitment of inflammatory eosinophils to the TME has been linked to anti-tumorigenic activity in a mouse model of breast cancer metastasis<sup>43</sup>. We hypothesize that these pro-inflammatory conditions induced intratumorally by  $T_{reg}$  depletion, may have contributed in combination with ICB to the development of a robust anti-metastatic immune response. In line with this hypothesis, we found that the combination of  $T_{reg}$  depletion and ICB induced a synergistic effect in the blood compartment on the mobilisation of  $CD8^+$  and  $CD4^+CD8^+$  T cells, NK cells, and additionally extended T cell activation. We speculate this may confer protection against circulating cancer cells or metastatic formation, leading to improved survival. Which of these anti-cancer mechanisms are most important to curb metastasis, and by which underlying immune cell crosstalk  $T_{regs}$  suppress anti-metastatic immunity, remains a topic of future research. Of note, the anti-tumoral effects of ICB + DT were only observed in the metastatic context, and not the primary tumor context. This suggests that additional hurdles for anti-tumor immunity are in place in primary KEP tumors, that are unrelated to  $T_{regs}$ . Previous research using the KEP model has shown that primary tumors are abundantly infiltrated by immunosuppressive neutrophils and macrophages<sup>44</sup> which may functionally suppress T cell function in absence of  $T_{regs}$ .

Our results concerning the adverse role of  $T_{regs}$  in the response to immunotherapy are consistent with clinical data which have revealed correlations between  $PD-1^+ T_{regs}$  and therapy response, relapse and hyper progressive disease in NCSLC, melanoma, and gastric cancer respectively<sup>16-18</sup>. Preclinical studies using inoculated B16 and MC38 cell line tumor models have shown that PD-1 blockade reactivates the proliferative and immunosuppressive capacity of  $PD-1^+ T_{regs}$ , thereby promoting tumor growth<sup>17,18</sup>. Furthermore, the efficacy of PD-1 blockade was shown to be dependent on high PD-1 expression on  $CD8^+$  T cells, but low PD-1 expression on  $T_{regs}$ <sup>17</sup>. In our study, we found that after discontinuation of treatment, the frequency of  $CD44^+$  and  $PD-1^+ T_{regs}$  is strongly increased in blood of mice that received neoadjuvant treatment of anti-PD-1/CTLA4. This suggests that ICB treatment itself plays an important role in the accumulation of  $PD-1^+ T_{regs}$ , which can negatively impact anti-tumor immunity as discussed above. It remains to be investigated whether ICB-induced PD-1 expression is caused by increased proliferation of  $T_{regs}$  upon anti-CTLA4<sup>19</sup> or anti-PD-1<sup>18</sup>, or whether increased PD-1 expression on  $T_{regs}$  is potentially a result of chronic TCR stimulation in the context of ICB. Nevertheless, understanding how ICB induces PD-1 expression on  $T_{regs}$  may support the development of immune checkpoint inhibitors that selectively activate conventional T cells, but not  $T_{regs}$ .

Finally, our data suggest that combining ICB with T<sub>reg</sub>-targeting strategies is a potential avenue to improve ICB responses in breast cancer. However, due to the critical role of T<sub>regs</sub> in upholding immune tolerance and thereby prevention of auto-immune related diseases, approaches that partially instead of fully deplete T<sub>regs</sub> may be more feasible for use in cancer patients including OX-40, CCR4 and CD25<sup>11,18,45</sup>. Promisingly, preliminary histopathological analysis (Fig. S2C, Table 1) in KEP tumor-bearing mice showed that immune-related pathology was not further exacerbated upon combination of ICB + T<sub>reg</sub> depletion, compared to T<sub>reg</sub> depletion alone. As this study provides proof-of-principle that T<sub>regs</sub> impair anti-tumor immunity in the context ICB, it will be crucial to identify how the variety of immunomodulatory drugs that are in clinical development will affect T<sub>reg</sub> activation beyond anti-PD-1/anti-CTLA4. Looking forward, this may contribute to improved clinical decision making regarding the use of T<sub>reg</sub>-activating immunomodulatory drugs in cancer patients with abundant intratumoral accumulation of T<sub>regs</sub>.

## MATERIAL AND METHODS

### Mice

Mice were kept in individually ventilated cages at the animal laboratory facility of the Netherlands Cancer Institute under specific pathogen free conditions. Food and water were provided *ad libitum*. All animal experiments were approved by the Netherlands Cancer Institute Animal Ethics Committee, and performed in accordance with institutional, national and European guidelines for Animal Care and Use. The study is compliant with all relevant ethical regulations regarding animal research.

The following genetically engineered mice have been used in this study: *Keratin14 (K14)-cre;Cdh1<sup>F/F</sup>;Trp53<sup>F/F22</sup>* and *Cdh1<sup>F/F</sup>;Trp53<sup>F/F</sup>;Foxp3<sup>GFP-DTR</sup>* mice (further referred to as *Foxp3<sup>GFP-DTR</sup>*). All mouse models were on FVB/n background, and genotyping was performed by PCR analysis on toe clips DNA as described<sup>22</sup>. Starting at 6-7 weeks of age, female mice were monitored twice weekly for the development of spontaneous mammary tumor development. Upon mammary tumor formation, perpendicular tumor diameters were measured twice weekly using a calliper. End-stage was defined as cumulative tumor burden of 225mm<sup>2</sup>, unless indicated otherwise.

### Intervention studies

Antibody treatments in tumor-bearing KEP mice were initiated at a tumor size of 50mm<sup>2</sup>, and at 2-4mm<sup>2</sup> in KEP transplantation experiments. Mice were randomly allocated to treatment groups upon presentation of palpable tumors, and were intraperitoneally injected twice weekly with ICB; 100 µg of anti-PD-1 (1 mg/mL in PBS, clone RMP1-14, BioXCell) and 100 µg of anti-CTLA4 (1 mg/mL in PBS, clone 9D9, BioXCell) or control; 100 µg rat

lgG2a (1 mg/mL in PBS, clone 2A3, BioXCell). Treatments were discontinued at cumulative tumor burden of 225mm<sup>2</sup> in the KEP model, or upon mastectomy for KEP transplantation experiments at indicated size. For depletion of T<sub>regs</sub>, DT or PBS (DT vehicle control) treatment was initiated at a tumor size of 6-9mm<sup>2</sup>. Mice were treated twice with 25 µg diphtheria toxin (Sigma) or PBS on day 0, and 4.

### Flow cytometry analysis and cell sorting

Draining lymph nodes and tumors were collected in ice-cold PBS, and blood was collected in heparin-containing tubes. Draining lymph nodes and tumors were processed as previously described<sup>46</sup>. Blood was obtained via cardiac puncture for end-stage analyses. Erythrocyte lysis for blood was performed in NH<sub>4</sub>Cl erythrocyte lysis buffer for 5 minutes. Single cell suspensions were incubated for 20 minutes with anti-CD16/32 (2.4G2, BD Biosciences) to block unspecific Fc receptor binding and fluorochrome conjugated antibodies diluted in FACS buffer (2.5% FBS, 2 mM EDTA in PBS). For analysis of intracellular proteins, cells were fixed and permeabilized after surface and live/dead staining using the FXP3 Transcription buffer set (ThermoFisher), according to manufacturer's instruction. Fixation, permeabilization and intracellular staining was performed for 30 minutes. Cell suspensions were analysed on a BD Symphony SORP or sorted on a FACS ARIA II (4 lasers). Absolute cell counts were determined using 123count eBeads (ThermoFisher) according to manufacturer's instruction. Single cell suspensions for cell sorting were prepared under sterile conditions. Sorting of T<sub>regs</sub> (Live, CD45<sup>+</sup>CD3<sup>+</sup>CD4<sup>+</sup>CD25<sup>+</sup> from indicated tissues and splenic responder cells (Live, CD45<sup>+</sup>CD3<sup>+</sup> → CD4<sup>+</sup>CD25<sup>-</sup> or CD8<sup>+</sup>) performed as previously described<sup>46</sup>. The following fluorochrome-conjugated antibodies were used in this study: CD3- BV421 (1:100), CD3-PECy7 (1:200), CD3-APC (1:400), CD4-APCeF780 (1:200), CD4-BV785 (1:400), CD4-PE (1:200), CD8-APC (1:200), CD8-BUV395 (1:200), CD8-FITC (1:400), CD11c-BUV737 (1:100), CD11b-BV786 (1:400), CD25-PE (1:200), CD25-APC (1:200), CD44-BV605 (1:200), CD45-BUV395 (1:200), CD45-BUV563 (1:400), CD62L-AF700 (1:200), CD62L-APCeF780 (1:200), CD69-BUV737 (1:200), CD101-PECy7 (1:200), CD103-APC (1:200), F4/80-BUV395 (1:200), FXP3-AF647 (1:100), Ki67-BV786 (1:200), Ly6C-eF450 (1:400), Ly6G-AF700 (1:200), MHC-II-FITC (1:200), NKp46-FITC (1:200), NKp46-PE (1:200), PD1-PECy7 (1:200), PDL1-PE (1:200), SiglecF-BV605 (1:200). Viability dyes: 7AAD (1:20), Fixable viability dye eFluor 780 (1:1000).

### KEP metastasis model

The KEP metastasis model has been applied as previously described<sup>23</sup>. Tumors from KEP mice (100mm<sup>2</sup>) were fragmented into small pieces (~1 mm<sup>2</sup>) and stored at -150 °C in Dulbecco's Modified Eagle's Medium F12 containing 30% fetal calf serum and 10% dimethyl sulfoxide. Selection of mouse invasive lobular carcinomas (mILC) donor tumors was based on high cytokeratin 8 and absence of vimentin and E-cadherin expression as determined by immunohistochemistry. Donor KEP tumor pieces were thawed, washed, and orthotopically transplanted into the 4<sup>th</sup> mammary fat pad of female recipient 8-16 week old

FOXP3<sup>DTR-GFP</sup> mice. Upon tumor outgrowth to a size of 100-150mm<sup>2</sup>, tumors were surgically removed. Following mastectomy, mice were monitored for development of overt multi-organ metastatic disease by daily palpation and observation of physical health, appearance, and behavior. Lungs, liver, spleen, intestines, kidneys, and tumor-draining (proper axillary and accessory axillary) lymph nodes were collected and analysed microscopically for the presence of metastatic foci by immunohistochemical cytokeratin 8 staining. Mice were excluded from analysis due to following predetermined reasons: No outgrowth of tumors upon transplantation, mice sacrificed due to surgery-related complications, mice sacrificed due to development of end-stage (225mm<sup>2</sup>) local recurrent tumors prior to presentation of metastatic disease, mice sacrificed due to metastasis-unrelated pathology.

### T<sub>reg</sub> suppression assays

T<sub>reg</sub>-T cell suppression assays were performed as previously described<sup>46</sup>. T<sub>regs</sub> (Live, CD45<sup>+</sup> CD3<sup>+</sup>, CD8<sup>-</sup> CD4<sup>+</sup>, CD25<sup>high</sup>) sorted from freshly isolated samples were activated overnight in IMDM containing 8% FCS, 100 IU/ml penicillin, 100 µg/ml streptomycin, 0.5% β-mercaptoethanol, 300U/mL IL-2, 1:5 bead:cell ratio CD3/CD28 coated beads (Thermofisher). Per condition, 2.5\*10<sup>4</sup> cells were seeded in 96-wells plate, which were further diluted to appropriate ratios (1:2 – 1:16. Responder cells (Live, CD45<sup>+</sup> CD3<sup>+</sup>, CD4<sup>+</sup>, CD25<sup>-</sup> and Live, CD45<sup>+</sup> CD3<sup>+</sup>, CD8<sup>+</sup>) were rested overnight. Next, responder cells were labelled with CellTraceViolet, and co-cultured with T<sub>regs</sub> in cIMDM supplemented with CD3/CD28 beads (1:5 bead cell ratio) for 96 hours (without exogenous IL-2).

### Immunohistochemistry

Immunohistochemical analyses were performed by the Animal Pathology facility at the Netherlands Cancer Institute. Formalin-fixed tissues were processed, sectioned and stained as described<sup>23</sup>. In brief, tissues were fixed for 24 h in 10% neutral buffered formalin, embedded in paraffin, sectioned at 4 µm and stained with haematoxylin and eosin (H&E) for inflammation-related histopathological evaluation by a trained animal pathologist. Slides were digitally processed using QuPath. For immunohistochemical analysis, 5-µm paraffin sections were cut, deparaffinized and stained. Brightness and contrast for representative images were adjusted equally among groups.

### Statistical analysis

Data analyses were performed using GraphPad Prism (version 8). Data show means ± SEM unless stated otherwise. The statistical tests used are described in figure legends. For comparison of two groups of continuous data, Student's T-test and Mann Whitney's T Test were used as indicated. For comparison of a single variable between multiple groups of normally distributed continuous data, we used one-way ANOVA, followed by indicated post-hoc analyses. For comparison of ≥2 variables between multiple groups, two-way ANOVA was used, followed by indicated post-hoc analyses. Fisher's exact test was used

to assess significant differences between categorical variables obtained from lymph node metastasis incidence. All tests were performed two-tailed. P-values < 0.05 were considered statistically significant. *In vivo* interventions were performed once with indicated sample sizes, unless otherwise indicated. *In vitro* experiments were repeated independently as indicated, Asterisks statistically significant differences. \* P < 0.05, \*\* P < 0.01, \*\*\* P < 0.001, \*\*\*\* P < 0.0001.

### **Author contributions**

K.Ko, L.S, O.B and K.E.d.V. conceived the ideas and designed the experiments. K.Ko, L.S, O.B performed experiments and data analysis. K.Ko, L.S, O.B, D.K., K.V, C.-S.H., L.R and K.Ke performed animal experiments. K.E.d.V. supervised the study, K.E.d.V and K.K acquired funding, K.K, L.S, O.B and K.E.d.V. wrote the paper and prepared the figures with input from all authors.

### **Acknowledgements**

We thank members of the Tumor Biology & Immunology Department, NKI for their insightful input. We thank the flow cytometry facility, animal laboratory facility, transgenesis facility and animal pathology facility of the Netherlands Cancer Institute for technical assistance. We thank Sjoerd Klaarenbeek for providing histopathological analysis.

### **Funding**

NWO Oncology Graduate School Amsterdam (OOA) Diamond Program (KK)  
Netherlands Organization for Scientific Research grant NWO-VICI 91819616 (KdV)  
Dutch Cancer Society grant KWF10083; KWF10623; KWF13191 (KdV)  
Oncode Institute (KdV)

### **Competing interests**

KdV reports research funding from Roche and is consultant for Macomics, outside the scope of this work.

### **Data availability**

Data are available from the authors on reasonable request.

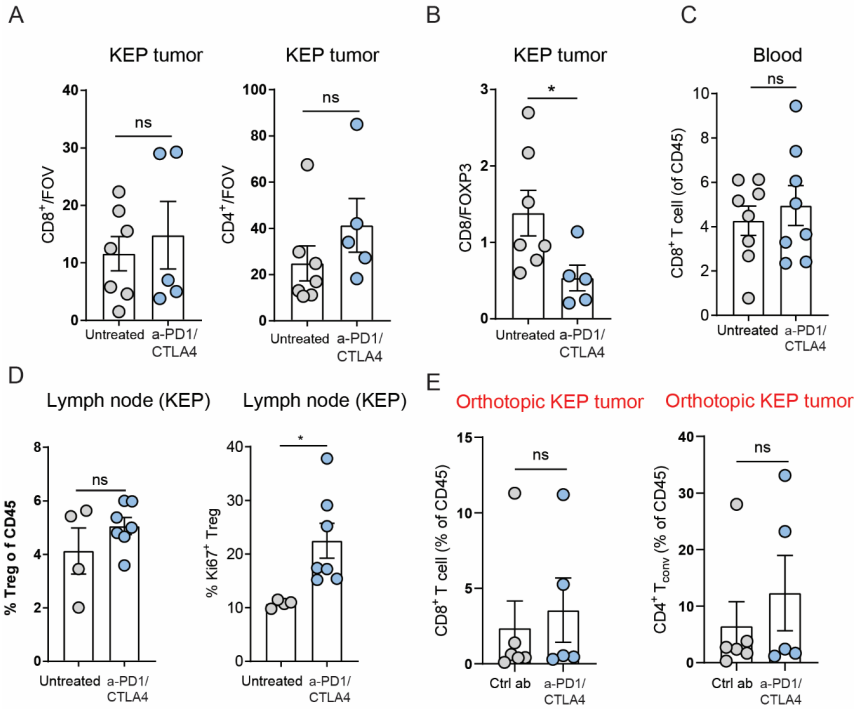
## REFERENCES

1. Blank, C. U. *et al.* Neoadjuvant versus adjuvant ipilimumab plus nivolumab in macroscopic stage III melanoma. *Nature Medicine* vol. 24 1655–1661 (2018).
2. Doroshow, D. B. *et al.* Immunotherapy in Non-Small Cell Lung Cancer: Facts and Hopes. *Clin. Cancer Res.* **25**, 4592–4602 (2019).
3. Chalabi, M. *et al.* Neoadjuvant immunotherapy leads to pathological responses in MMR-proficient and MMR-deficient early-stage colon cancers. *Nat. Med.* **2020** *264* **26**, 566–576 (2020).
4. Sharma, P., Hu-Lieskovan, S., Wargo, J. A. & Ribas, A. Leading Edge Review Primary, Adaptive, and Acquired Resistance to Cancer Immunotherapy. (2017) doi:10.1016/j.cell.2017.01.017.
5. Adams, S. *et al.* Pembrolizumab monotherapy for previously untreated, PD-L1-positive, metastatic triple-negative breast cancer: Cohort B of the phase II KEYNOTE-086 study. *Ann. Oncol.* **30**, 405–411 (2019).
6. Dirix, L. Y. *et al.* Avelumab, an anti-PD-L1 antibody, in patients with locally advanced or metastatic breast cancer: A phase 1b JAVELIN solid tumor study. *Breast Cancer Res. Treat.* **167**, 671–686 (2018).
7. Chen, D. S. & Mellman, I. Oncology Meets Immunology: The Cancer-Immunity Cycle. *Immunity* **39**, 1–10 (2013).
8. Simon, S. & Labarriere, N. PD-1 expression on tumor-specific T cells: Friend or foe for immunotherapy? <https://doi.org/10.1080/2162402X.2017.1364828> **7**, (2017).
9. Tanaka, A. & Sakaguchi, S. Regulatory T cells in cancer immunotherapy. *Cell Research* vol. 27 109–118 (2017).
10. Sharpe, A. H. & Pauken, K. E. The diverse functions of the PD1 inhibitory pathway. *Nat. Rev. Immunol.* **18**, 153–167 (2018).
11. Plitas, G. & Rudensky, A. Y. Regulatory T Cells in Cancer. *Annu. Rev. Cancer Biol.* **4**, 459–477 (2020).
12. Kos, K. & de Visser, K. E. The Multifaceted Role of Regulatory T Cells in Breast Cancer. *Annu. Rev. Cancer Biol.* **5**, (2021).
13. Bos, P. D., Plitas, G., Rudra, D., Lee, S. Y. & Rudensky, A. Y. Transient regulatory T cell ablation deters oncogene-driven breast cancer and enhances radiotherapy. *J. Exp. Med.* **210**, 2435–2466 (2013).
14. Clark, N. M. *et al.* Regulatory T Cells Support Breast Cancer Progression by Opposing IFN- $\gamma$ -Dependent Functional Reprogramming of Myeloid Cells. *Cell Rep.* **33**, (2020).
15. Kos, K. *et al.* Tumor-educated Tregs drive organ-specific metastasis in breast cancer by impairing NK cells in the lymph node niche. *Cell Rep.* **38**, 110447 (2022).
16. Huang, A. C. *et al.* A single dose of neoadjuvant PD-1 blockade predicts clinical outcomes in resectable melanoma. *Nat. Med.* **25**, 454–461 (2019).
17. Kumagai, S. *et al.* The PD-1 expression balance between effector and regulatory T cells predicts the clinical efficacy of PD-1 blockade therapies. *Nat. Immunol.* **21**, 1346–1358 (2020).
18. Kamada, T. *et al.* PD-1(+) regulatory T cells amplified by PD-1 blockade promote hyperprogression of cancer. *PNAS* **116**, 9999–10008 (2019).
19. Marangoni, F. *et al.* Expansion of tumor-associated Treg cells upon disruption of a CTLA-4-dependent feedback loop. *Cell* **184**, 3998–4015.e19 (2021).
20. Kavanagh, B. *et al.* CTLA4 blockade expands FoxP3+ regulatory and activated effector CD4+ T cells in a dose-dependent fashion. *Blood* **112**, 1175 (2008).
21. Sharma, A. *et al.* Anti-CTLA-4 immunotherapy does not deplete Foxp3  $\beta$  regulatory T cells (Tregs) in human cancers. *Clin. Cancer Res.* **25**, 1233–1238 (2019).
22. Derksen, P. W. B. *et al.* Somatic inactivation of E-cadherin and p53 in mice leads to metastatic lobular mammary carcinoma through induction of anoikis resistance and angiogenesis. *Cancer Cell* **10**, 437–449 (2006).
23. Doornebal, C. W. *et al.* A Preclinical Mouse Model of Invasive Lobular Breast Cancer Metastasis. *Cancer Res.* **73**, 353 LP – 363 (2013).
24. Tavares, M. C. *et al.* A high CD8 to FOXP3 ratio in the tumor stroma and expression of PTEN in tumor cells are associated with improved survival in non-metastatic triple-negative breast carcinoma. *BMC Cancer* **21**, 901 (2021).
25. Kim, J. M., Rasmussen, J. P. & Rudensky, A. Y. Regulatory T cells prevent catastrophic autoimmunity throughout the lifespan of mice. *Nat. Immunol.* **8**, 191–7 (2007).
26. Wang, S., Shen, H., Bai, B., Wu, J. & Wang, J. Increased CD4+CD8+Double-Positive T Cell in Patients with Primary Sjögren's Syndrome Correlated with Disease Activity. *J. Immunol. Res.* **2021**, (2021).
27. Parel, Y. *et al.* Presence of CD4+CD8+ double-positive T cells with very high interleukin-4 production potential in lesional skin of patients with systemic sclerosis. *Arthritis Rheum.* **56**, 3459–3467 (2007).
28. Bohner, P. *et al.* Double positive CD4+CD8+ T cells are enriched in urological cancers and favor T helper-2 polarization. *Front. Immunol.* **10**, 622 (2019).

29. Desfrançois, J. *et al.* Double Positive CD4CD8  $\alpha\beta$  T Cells: A New Tumor-Reactive Population in Human Melanomas. *PLoS One* **5**, (2010).
30. Kim, J. M., Rasmussen, J. P. & Rudensky, A. Y. Regulatory T cells prevent catastrophic autoimmunity throughout the lifespan of mice. *Nat. Immunol.* **8**, 191–197 (2007).
31. Liu, J. *et al.* Assessing immune-related adverse events of efficacious combination immunotherapies in preclinical models of cancer. *Cancer Res.* **76**, 5288–5301 (2016).
32. Carretero, R. *et al.* Eosinophils orchestrate cancer rejection by normalizing tumor vessels and enhancing infiltration of CD8 + T cells. *Nat. Immunol.* **16**, 609–617 (2015).
33. Binnewies, M. *et al.* Unleashing Type-2 Dendritic Cells to Drive Protective Antitumor CD4+ T Cell Immunity. *Cell* **177**, 556–571.e16 (2019).
34. Pan, Y., Yu, Y., Wang, X. & Zhang, T. Tumor-Associated Macrophages in Tumor Immunity . *Frontiers in Immunology* vol. 11 3151 (2020).
35. Levine, A. G., Arvey, A., Jin, W. & Rudensky, A. Y. Continuous requirement for the TCR in regulatory T cell function. *Nat. Immunol.* **15**, 1070–1078 (2014).
36. Davis, A. A. & Patel, V. G. The role of PD-L1 expression as a predictive biomarker: an analysis of all US Food and Drug Administration (FDA) approvals of immune checkpoint inhibitors. *J. Immunother. Cancer* **7**, 278 (2019).
37. Hollande, C. *et al.* Inhibition of the dipeptidyl peptidase DPP4 (CD26) reveals IL-33-dependent eosinophil-mediated control of tumor growth. *Nat. Immunol.* **20**, 257–264 (2019).
38. Zhang, F. *et al.* Genetic programming of macrophages to perform anti-tumor functions using targeted mRNA nanocarriers. *Nat. Commun.* 2019 101 **10**, 1–16 (2019).
39. Waldman, A. D., Fritz, J. M. & Lenardo, M. J. A guide to cancer immunotherapy: from T cell basic science to clinical practice. *Nat. Rev. Immunol.* 2020 2011 **20**, 651–668 (2020).
40. Zheng, X. *et al.* CTLA4 blockade promotes vessel normalization in breast tumors via the accumulation of eosinophils. *Int. J. cancer* **146**, 1730–1740 (2020).
41. Akuthota, P., Wang, H. & Weller, P. F. Eosinophils as Antigen-Presenting Cells in Allergic Upper Airway Disease. *Curr. Opin. Allergy Clin. Immunol.* **10**, 14 (2010).
42. Simon, S. C. S. *et al.* Eosinophil accumulation predicts response to melanoma treatment with immune checkpoint inhibitors. *Oncoimmunology* **9**, (2020).
43. Grisaru-Tal, S. *et al.* Metastasis-Entrained Eosinophils Enhance Lymphocyte-Mediated Antitumor Immunity. *Cancer Res.* **81**, 5555–5571 (2021).
44. Salvagno, C. *et al.* Therapeutic targeting of macrophages enhances chemotherapy efficacy by unleashing type I interferon response. *Nat. Cell Biol.* **21**, 511–521 (2019).
45. Solomon, I. *et al.* CD25-Treg-depleting antibodies preserving IL-2 signaling on effector T cells enhance effector activation and antitumor immunity. *Nat. Cancer* 2020 112 **1**, 1153–1166 (2020).
46. Kos, K., van Baalen, M., Meijer, D. A. & de Visser, K. E. Flow cytometry-based isolation of tumor-associated regulatory T cells and assessment of their suppressive potential. in *Methods in Enzymology* (2019). doi:10.1016/bs.mie.2019.07.035.



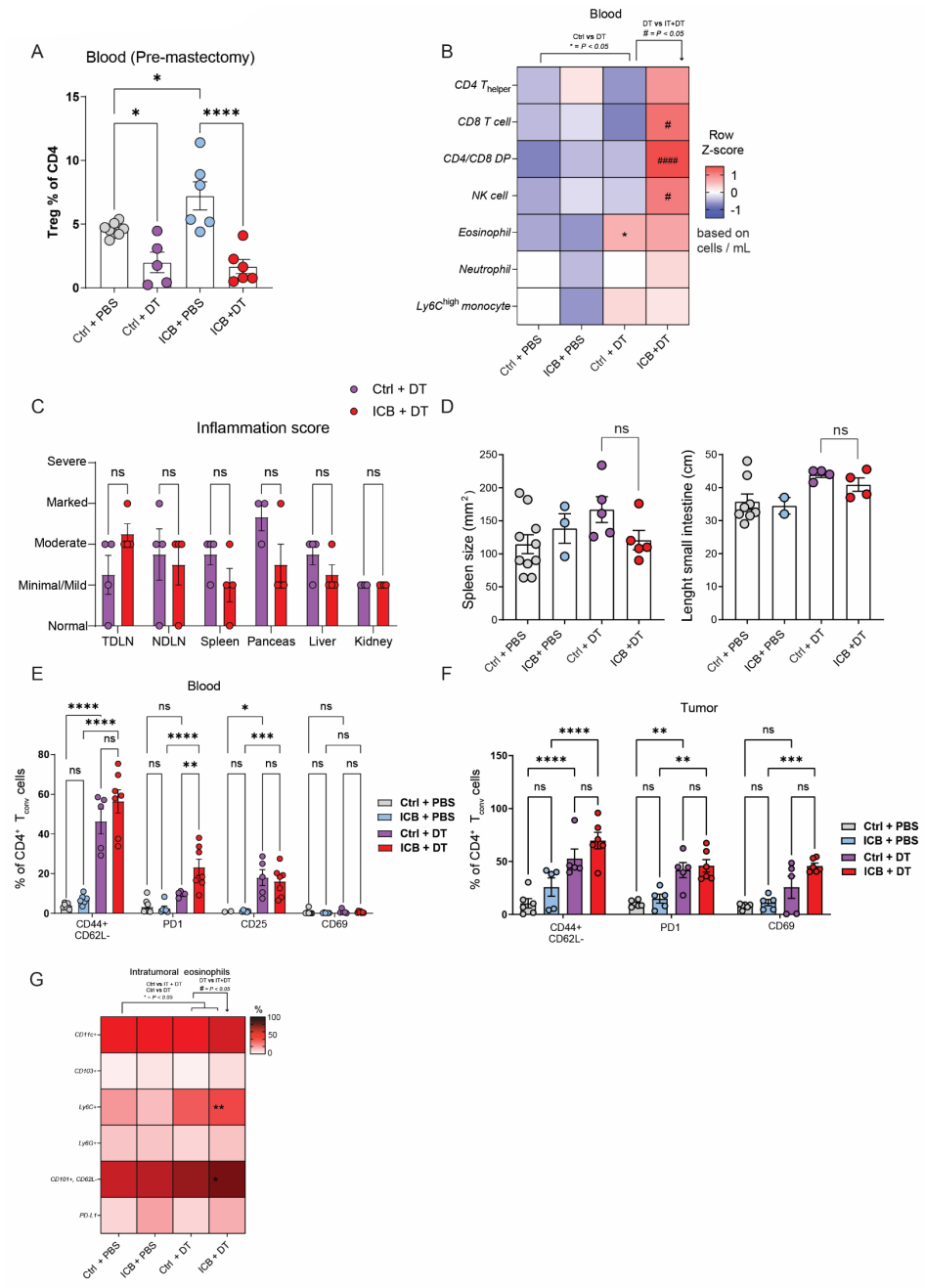
**SUPPLEMENTARY MATERIAL**



**SUPPLEMENTAL FIGURE 1. Effect of ICB on intratumoral and systemic T cell accumulation in tumor-bearing KEP mice**

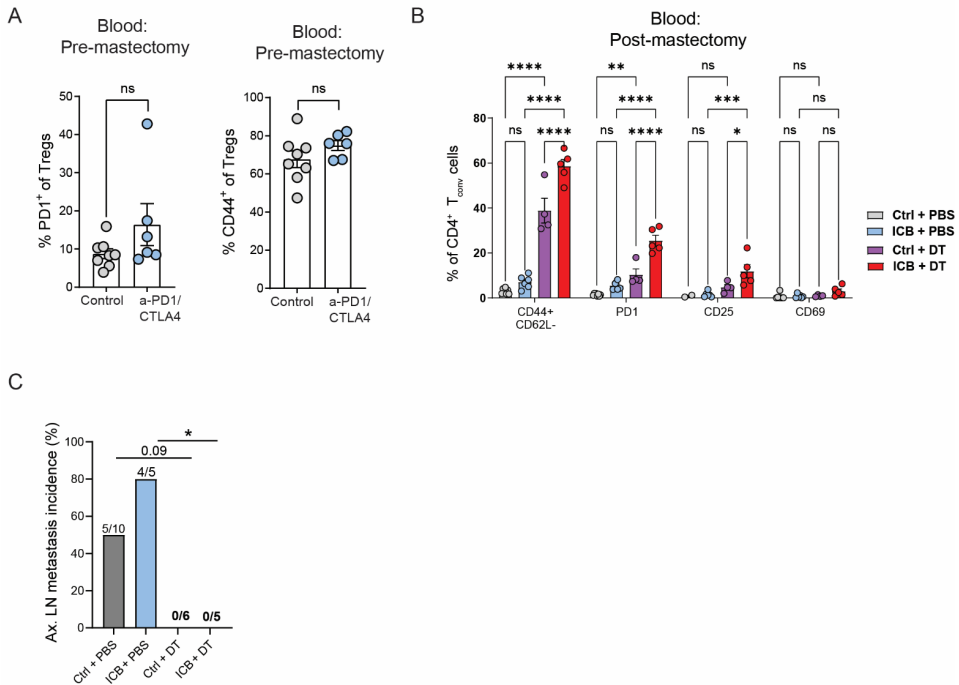
CD8 (left) and CD4 (right) counts in spontaneous mammary tumors (225mm<sup>2</sup>) of KEP mice treated as indicated, as determined by immunohistochemical analysis (counts per 40x field of view, average of five randomly selected areas) (n=5-7 mice/group). **B**. Ratio of CD8 and FOXP3 counts shown in Fig. 1D and S1A. **C**. Frequency of CD8<sup>+</sup> T cells as % of total live CD45<sup>+</sup> cells in blood of KEP mice bearing mammary tumors (225mm<sup>2</sup>), treated with control or anti-PD-1/CTLA4 (n=8 mice/group). **D**. Quantification of T<sub>regs</sub> as % of total live CD45<sup>+</sup> cells (left) and frequency of Ki-67 expression (right) on T<sub>regs</sub> (CD4<sup>+</sup>CD25<sup>+</sup>), and in lymph nodes isolated from KEP mice bearing mammary tumors (225mm<sup>2</sup>), treated as indicated (n=4-7 mice/group). **E**. Frequency of CD8<sup>+</sup> (left) and CD4<sup>+</sup>CD25<sup>-</sup> (right) T cells as % of total live CD45<sup>+</sup> cells in orthotopically transplanted KEP tumors (100-150mm<sup>2</sup>) of mice treated with control antibody, or anti-PD-1/CTLA4, as analysed by flow cytometry (n=4-7 mice/group).

Data in A-E show mean ± SEM. P-values were calculated by Student's T-test. \* P < 0.05, \*\* P < 0.01, \*\*\* P < 0.001, \*\*\*\* P < 0.0001.



**SUPPLEMENTAL FIGURE 2. Pre-mastectomy analysis of the effect of T<sub>reg</sub> depletion in the context of ICB on blood and tumors of KEP tumor-bearing mice:**

**A.** Frequency of T<sub>regs</sub> (defined as CD4<sup>+</sup>GFP<sup>+</sup> in Ctrl + DT, ICB + PBS, ICB + DT or CD4<sup>+</sup>CD25<sup>+</sup> in Ctrl + PBS) in blood of mice treated with indicated treatments, as determined by flow cytometry 1-2 days before mastectomy (n=5-8 mice/group). **B.** Heatmap depicting immune landscape in blood of mice receiving indicated treatments, as determined by flow cytometry 1-2 days before mastectomy. Row Z-score calculated based on absolute cell counts of indicated cell type per mL of blood (n=6-8 mice/group). **C.** Histopathological assessment of inflammation-related pathology in various organs of mice treated as indicated as analysed blindly by a trained animal pathologist. Scoring based on data shown in Table 1. **D.** Size of spleen (left) and small intestine (right) of mice treated as indicated. **E.** Frequency of indicated markers gated on CD4<sup>+</sup>T<sub>conv</sub> cells in blood of mice treated as indicated, determined by flow cytometry, pre-mastectomy (n=2-8 mice/group). **F.** Frequency on indicated markers on gated CD4<sup>+</sup>T<sub>conv</sub> cells in mastectomized tumors of mice treated as indicated, determined by flow cytometry, pre-mastectomy (n=5-6 mice/group). **G.** Heatmap depicting expression of indicated markers on eosinophils in mastectomized tumors of mice receiving indicated treatments (n=5-6 mice/group). Data in A,E,F show mean ± SEM. P-values were calculated using One-way ANOVA with Sidak's correction (A,B,D,G), 2-way ANOVA with Sidak's correction (C,E,F).



**SUPPLEMENTAL FIGURE 3. Post-mastectomy analysis of the effect of T<sub>reg</sub> depletion in the context of ICB on blood and tumors of KEP tumor-bearing mice:**

**A.** Frequency of PD-1 (left) and CD44 (right) expression on T<sub>regs</sub> (CD4<sup>+</sup>CD25<sup>+</sup>) in blood of mice 1-2 days before mastectomy, treated as indicated (n=6-8 mice group). **B.** Expression of indicated markers on CD4<sup>+</sup>T<sub>conv</sub> cells in blood of mice 7 days after mastectomy, previously treated as indicated (n=6-8 mice group). **C.** % and number of mice with metastases in axillary TDLNs in mice treated as indicated, as determined by immunohistochemical analysis of keratin 8 staining. Data in A,B show mean ± SEM. P-values were calculated using Student's T-test (A), 2-way ANOVA with Sidak's correction (B), Fisher's Exact Test (C). \* P < 0.05, \*\* P < 0.01, \*\*\* P < 0.001, \*\*\*\* P < 0.0001.